Power System Technology
ISSN:1000-3673

Received: 02-11-2025 Revised: 12-12-2025 Accepted: 27-12-2025

Design and Simulation of a $Cs_2AgBiBr_6/PbS-TBAI$ Dual-Absorber Hybrid Solar Cell using SCAPS-1D

Satyabrat Pandey[1,*], Brijesh Kumar Pandey[1], Km Pragya Mishra[1], Hemant Kumar Dubey[2], Ratan Lal Jaiswal[3]

[1]Department of Physics and Material Science, Madan Mohan Malaviya University of Technology, Gorakhpur (U.P.) India.

[2]Department of Chemistry, Baba Raghav Das Post Graduate College, Deoria, (U.P.) India

[3]Department of Physics, Government Degree College Dhadha Buzurg Hata, Kuishinagar (U.P.) India

*Corresponding author e-mail: satyabratbrdpg@gmail.com

Abstract

A double perovskite, $Cs_2AgBiBr_6$-based solar cells have attracted considerable attention due to their promising efficiency, along with their stability and earth-abundant composition. At the same time, PbS–TBAI has emerged as a high-performing quantum dot material, demonstrating strong potential for photovoltaic applications. In this study, we investigate a hybrid solar cell that combines both of these absorber materials. The primary absorber layer is PbS–TBAI, while PCBM is employed as the electron transport layer (ETL) and Cu_2O as the hole transport layer (HTL). For further extension the absorption range and support overall light harvesting, two materials having different bandgap can enhance the absorption. A double perovskite $Cs_2AgBiBr_6$ layer is integrated with PbS–TBAI. The inclusion of this secondary absorber leads to a notable improvement in device performance, achieving an efficiency of 27.90% with an open-circuit voltage of 0.8665 V, a short-circuit current density of 40.68 mA cm^{-2}, and a fill factor of 79.16%. The optimization process was carried out by varying the thicknesses of both absorber layers, as well as analyzing the effect of interface defect density at the $Cs_2AgBiBr_6/PbS-TBAI$ junction. In addition, the doping densities of the ETL and HTL were carefully adjusted to refine the device architecture.

Keywords: Quantum dot, solar cell, Affordable and clean energy, MEG, Dual absorber layer, $Cs_2AgBiBr_6/PbS-TBAI$

1. Introduction

Energy is the cornerstone of modern civilization, and new research in energy production is advancing at an unprecedented pace. Solar energy is both an appealing and plentiful source, easily found in the form of light worldwide. Renewable energy can be captured and converted into a versatile form of energy: electrical energy. A solar cell (SC) uses the photovoltaic effect to convert radiation into electricity[1], [2], [3].

Solar cells are broadly categorized into three generations based on the materials used and the underlying technology. The first generation primarily consists of silicon-based solar cells, which

Power System Technology
ISSN:1000-3673
Received: 02-11-2025 Revised: 12-12-2025 Accepted: 27-12-2025

remain the most widely deployed in the commercial sector. These cells are valued for their long-term stability and reliability, though their fabrication involves significant costs. They have achieved efficiencies of up to 26.6%[3], [4]. Despite the emergence of new materials, silicon technology continues to dominate the market as no true alternative has yet matched its balance of efficiency, durability, and scalability.

The second generation includes thin-film solar cells, which are designed to reduce material usage and manufacturing costs. Their active layers are only a few micrometers thick, making them lightweight and flexible, while also offering potential for large-scale production. Reported efficiencies are around 22%[5][3], which is close to that of silicon devices. However, commercialization has been limited due to the complexity of the fabrication process and the reliance on scarce elements such as indium and tellurium. These challenges have restricted their widespread adoption despite their promising attributes. It is also important to note that the efficiency of single-junction solar cells is fundamentally constrained by the Shockley–Queisser (S-Q) limit, which sets the theoretical maximum efficiency under standard illumination conditions which is 33.7% because of various losses, such as thermal losses, transmission losses and recombination losses. This means that around 66% of incoming light energy is lost[3], [6].

The aim of ongoing research is to overcome the S-Q limit as well as to reduce the cost of production, and this can be done if excess energy from light, as well as low-energy photons, utilized effectively. The quantum dots are magical nanoparticles that have both the properties of absorbing high-energy and low-energy photons. The main materials of third generation are Perovskite and Quantum dots[7], [8], [9], [10]. Perovskite material has its stability issues, and so quantum dots are now of leading interest because of their special tunable optical properties and stability. QD semiconductors are spherical nanomaterial with a size of a few 10 nm. Out of QD materials, PbS QD is most suitable as it is stable, easy to prepare, low-cost, low-temperature synthesis, scalable fabrication at large scales, and has an appropriate band gap of 0.7–1.5 eV[9], [11]. Its quantum efficiency is good in the IR region. The solar spectrum has 49% IR, 46% Visible, and 5% UV radiation[12]. A QD solar cell has quantum efficiency (QE) because of low-energy photons are absorbed directly, and high-energy radiation generates hot electrons, which further generate electrons. This is called multiple-exciton generation and is also a phenomenal property found in QDs[13]. Since quantum efficiency of this cell is good in the IR region[14], this shows that the cell performance will not degrade too much in the evening or cloudy weather[15]. This positions PbS QD solar cells among the leading third-generation photovoltaic technologies[16]. This SC can also be combined with other types of materials with different band-gap to broaden the light absorption spectrum[17]. Now, Perovskite is a promising material with a low cost of fabrication and a good range of band gap, so it is resulted in a beautiful material of attraction for the researchers looking for the development of the SC in succession[18]. Here, this precious knowledge of materials is used to design an architecture that solves the problems of low efficiency as well as good fill factor and other parameters. SCAPS 1D is the tool that enables us to design the architecture based on assumptions and ideas drawn forward for the development of SC in our capacity, and some conclusions are drawn[19][20].

Power System Technology
ISSN:1000-3673
Received: 02-11-2025 Revised: 12-12-2025 Accepted: 27-12-2025

In this design, an additional perovskite absorber layer with a complementary band gap is integrated with the PbS quantum dot absorber to harvest photons that remain unabsorbed by the first layer. This spectral complementarity enables more efficient utilization of the solar spectrum, leading to a significant enhancement in overall device performance. The resulting improvement in photovoltaic parameters demonstrates the strong potential of perovskite–PbS quantum dot dual-absorber architectures and provides clear motivation for experimental realization[21], [22], [23]. This work seeks to identify more appropriate layers of HTL and ETL for better efficiency in colloidal quantum dot (CQD) solar cells, as well as to add some additional layers to support the absorption of incident light [24]. For this, SCAPS 1D software is used to simulate the idea. This software is well-known in the field of solar cells and is widely used by researchers. Here, the roles of different layers are studied, series and shunt resistance are kept off, and the AM 1.5 solar spectrum is used as an incident light. The present work considers earlier work done by Priyanka Dubey et al. that has the structure $ITO/WO_3/PbS-TBAI/Cu_2O$ and has an efficiency of 23.05% [25]. Since there is always scope for improvement in the work by choosing suitable ETL and HTL material, and with some new idea of two absorber layers of different materials this work comes into view. Firstly, the earlier work is reproduced, and the tool is calibrated [26]. A new layer of Double Perovskite $Cs_2AgBiBr_6$ with a 1.61 eV band gap is introduced to absorb the photons that may leave the QD absorber layer [27]. A favorable device performance is obtained and subsequently analyzed by systematically varying the electron transport layer (ETL) and hole transport layer (HTL) within the proposed device architecture. Among the materials investigated, PCBM emerges as the most suitable ETL, while Cu_2O is identified as the optimal HTL. The superior performance of PCBM compared to WO_3 arises from its lower band gap and more favorable energy-level alignment with the PbS–TBAI absorber layer, which facilitates efficient electron extraction and transport. In addition, the energy offset at the ITO/PCBM interface effectively suppresses hole transport toward the front contact, thereby reducing recombination losses and contributing to an overall improvement in device efficiency. Quantum dots can absorb photons with energies that are multiples of their band gap (1.14 eV). The perovskite layer used in this study has a intermideate band gap of 1.61 eV. Together, these absorbers extend the overall absorption range. This combination may also improve device stability.

2. Methodology and Device Architecture

The proposed solar cell device is structured on a glass substrate and incorporates several functional layers in sequence. These include an indium tin oxide (ITO) layer, a PCBM-based electron transport layer (ETL), a PbS-TBAI colloidal quantum dot (CQD) absorber, a $Cs_2AgBiBr_6$ double perovskite absorber, and a Cu_2O hole transport layer (HTL). The complete architecture, along with the corresponding band gap alignment, is illustrated in Fig. 1.

Power System Technology
ISSN:1000-3673
Received: 02-11-2025 Revised: 12-12-2025 Accepted: 27-12-2025

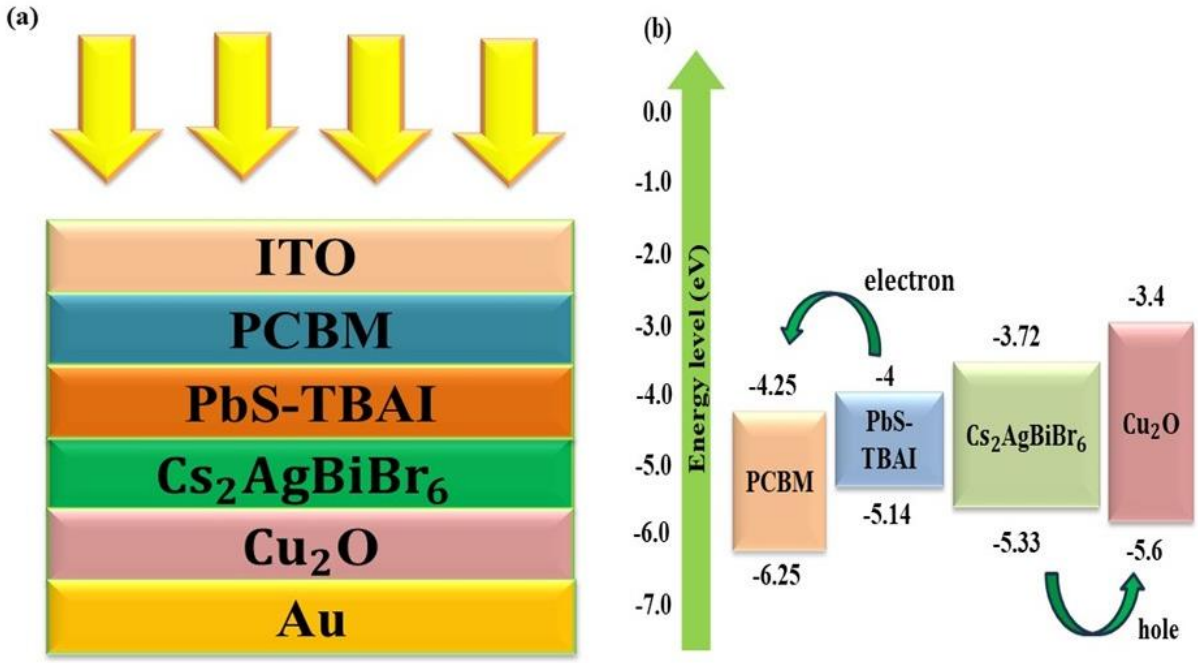

Fig. 1 Schematic diagram of the device architecture and its band gap.

Within this configuration, the HTL facilitates the extraction and transport of holes from the absorber layers, while the ETL collects photogenerated electrons and directs them efficiently towards the electrode. The performance of this architecture was evaluated using calibrated simulations carried out in the SCAPS-1D software (Solar Cell Capacitance Simulator). This computational tool is widely applied in photovoltaic research and operates on the basis of three coupled differential equations, namely Poisson's equation and the continuity equations for electrons and holes. These equations allow for an accurate description of charge transport, recombination, and electrostatic behaviour within the multilayer device structure.

$$\frac{d}{dx}\left(-\epsilon(x)\frac{d\emptyset}{dx}\right) = [p(x) - n(x) + N_D(x) - N_A(x) + p(x) - n(x)] \quad (1)$$

Here, p signifies hole density, and N_A , N_D signify the acceptor and donor densities, respectively. The electron density and trapped hole are denoted by n(x) and p(x), respectively, while the relative permittivity is denoted by $\epsilon(x)$.

$$\frac{\partial n(x,t)}{\partial x} = \frac{1}{q}\frac{\partial J_n}{\partial x} + G_n - R_n(x,t) \quad (2)$$

$$-\frac{\partial p(x,t)}{\partial x} = \frac{1}{q}\frac{\partial J_p}{\partial x} + G_p(x,t) - R_p(x,t) \quad (3)$$

where J_n and J_p are the current densities of electron and hole carriers, $R_{n.p}$ is the net recombination rate, and G is the electron-hole generation rate.

Power System Technology
ISSN:1000-3673
Received: 02-11-2025 Revised: 12-12-2025 Accepted: 27-12-2025

The drift diffusion equations are given by:

$$J_n = q\left[nu_nE + D_n\frac{dn}{dx}\right] \quad (4)$$

$$J_p = q\left[pu_pE - D_p\frac{dp}{dx}\right] \quad (5)$$

Where u_n, u_p are the electron and hole mobility, and D_n, D_p are the electron and hole diffusion coefficients. The band gap (E_g), the electron affinity, dielectric relative permittivity, effective density of states of conduction and valence band, acceptor and doping concentration, electron and hole mobility, Defect density, and the work function of the solar cell all have an impact on the performance parameters (V_{oc}, J_{sc}, FF, η) of the solar cell.

3. Simulation implementation and layer parameters

Figure 2 (a) demonstrates the band alignment improvement after addition of second absorber layer thus act as buffer layer too. This support the wider range absorption as well as charge transport mechanism. The Fig. 2 (b) shows the band alignment before second absorber layer addition, here the V_{bo} is more enough which affect charge transportation.

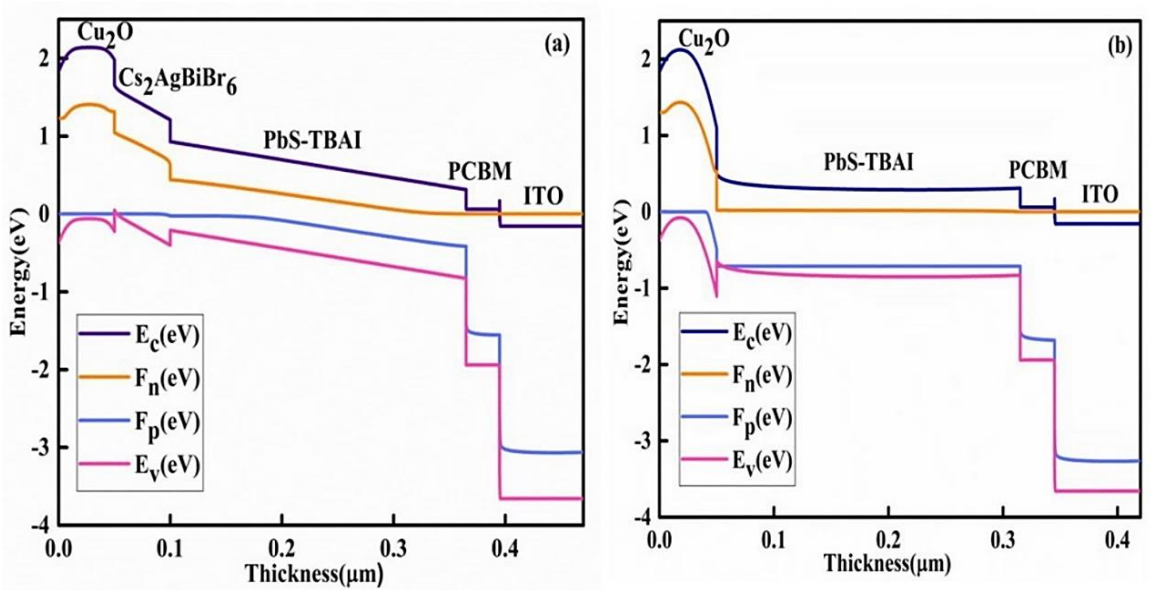

Fig. 2 Energy Band Diagram of the Architecture **(a)** Energy band diagram with second absorber **(b)** Energy band diagram with single absorber layer

In the Table 1, E_g is the band gap energy, χ is the electron affinity, ε_r is the Relative permittivity, μ_n, and $\mu_p$and are the mobility of the electron and hole, respectively. N_c , and N_v denote the effective density of states of the conduction and valence bands. N_A and N_D denote acceptor and donor density, respectively, and N_t is the defect density.

Power System Technology
ISSN:1000-3673
Received: 02-11-2025 Revised: 12-12-2025 Accepted: 27-12-2025

Table.1. Material parameters used in the calibration [33][34][35][36]

Parameters	**ITO**	**PCBM**	**PbS-TBAI**	**$Cs_2AgBiBr_6$**	**Cu_2O**
Thickness (nm)	80	30	265	50	50
$E_g(eV)$	3.5	2	1.14	1.61	2.2
$\chi(eV)$	4	4.250	4	3.72	3.4
ε_r	9	4	20	5.8	7.5
$\mu_n(cm^2/Vs)$	20	0.02	20	9.28	200
$\mu_p(cm^2/Vs)$	10	0.02	10	9.28	8.6×10^3
$N_c\ (cm^{-3})$	2.2×10^{18}	10^{21}	2×10^{18}	2×10^{18}	2×10^{19}
$N_v\ (cm^{-3})$	1.8×10^{19}	2×10^{20}	10^{18}	10^{18}	10^{19}
$N_D(cm^{-3})$	10^{21}	10^{20}	10^{15}	0	0
$N_A(cm^{-3})$	0	0	10^{15}	10^{15}	10^{18}
$N_t(cm^{-3})$	10^{14}	10^{14}	10^{14}	10^{14}	10^{14}

Using the Au work-function (5.1 eV), and the thermal velocities of electrons and holes are set as (10^7 cm/s). For the light spectrum, AM 1.5 and an operating temperature of 300 K were chosen and the defect parameters used for calibration are set to default.

4. J-V curve and Absorption curve of the proposed device

The J–V characteristics, with and without the incorporation of a second absorber layer, indicate that the open-circuit voltage (V_{oc}) remains nearly unchanged in both configurations. However, the fill factor (FF) improves significantly, suggesting that the device architecture more closely approaches the behavior of an ideal solar cell. The absorption profile (Fig. 3) demonstrates the spectral range captured by the different absorber layers. Specifically, PbS–TBAI exhibits absorption up to ~1100 nm, while $Cs_2AgBiBr_6$ absorbs efficiently up to ~800 nm. When combined, these absorbers complement each other, resulting in enhanced photon harvesting across a broader spectral range. Consequently, the external quantum efficiency (EQE) exceeds 90% over a wide portion of the spectrum, highlighting the effectiveness of the dual-absorber.

Power System Technology
ISSN:1000-3673
Received: 02-11-2025 Revised: 12-12-2025 Accepted: 27-12-2025

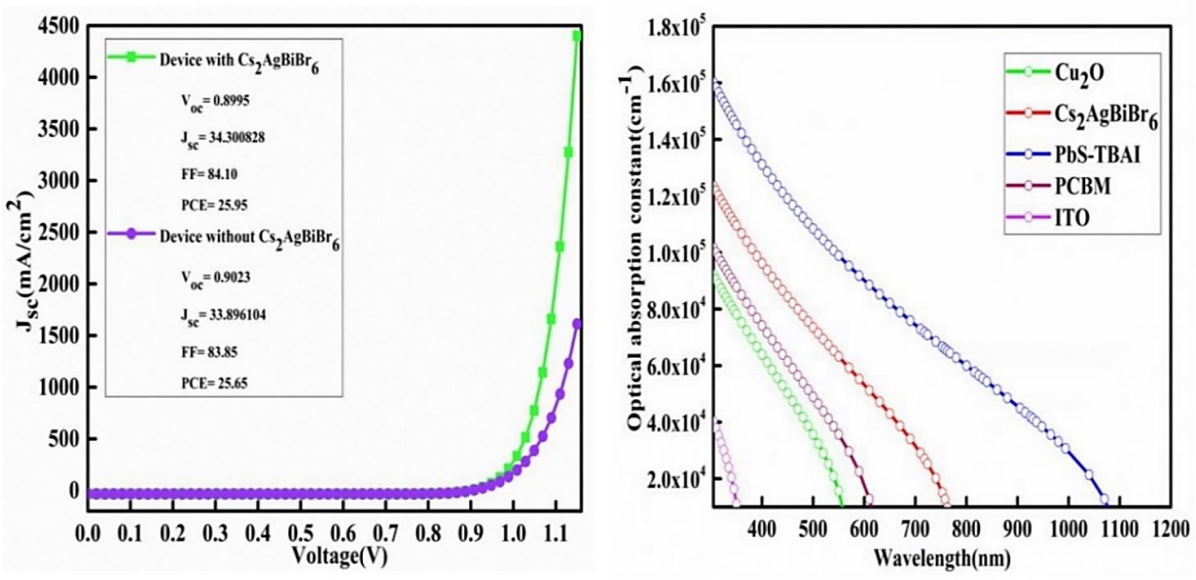

Fig. 3 Shows the J-V curve of Device with and without $Cs_2AgBiBr_6$and optical absorption of the materials.

5. Results and Discussion

5.1 Study of variation in thickness of the first absorber layer, PbS-TBAI

The fundamental operation of a solar cell relies on the absorption of photons to generate electron–hole pairs[37]. Therefore, the choice of absorber material is critical, as it must be capable of harvesting the maximum possible fraction of the solar spectrum. To achieve this, the solar spectrum is carefully studied in relation to the optical and electronic properties of potential absorber materials[38]. However, the intrinsic band gap of each material restricts absorption to photons with specific energies, thereby imposing a fundamental limit on device performance[6] [39]. Quantum dot materials offer a distinctive advantage in this context, as they can absorb not only photons with energies equal to their band gap but also those corresponding to integral multiples of it through multiple-exciton generation[7]. This unique property enhances overall photon utilization. Nonetheless, a single absorber layer cannot capture the full range of incident photons. To address this limitation, an additional absorber with an intermediate band gap can be introduced, enabling absorption of photons with slightly higher energies than those captured by the primary layer[40]. This dual-layer strategy improves light harvesting and device performance while simultaneously reducing hot-carrier thermalization losses, thereby contributing to enhanced operational stability[41].

In this study, the effect of absorber layer thickness on device performance was systematically investigated, with thickness values varied between 0.1 μm and 1 μm (Fig. 4).

Power System Technology
ISSN:1000-3673
Received: 02-11-2025 Revised: 12-12-2025 Accepted: 27-12-2025

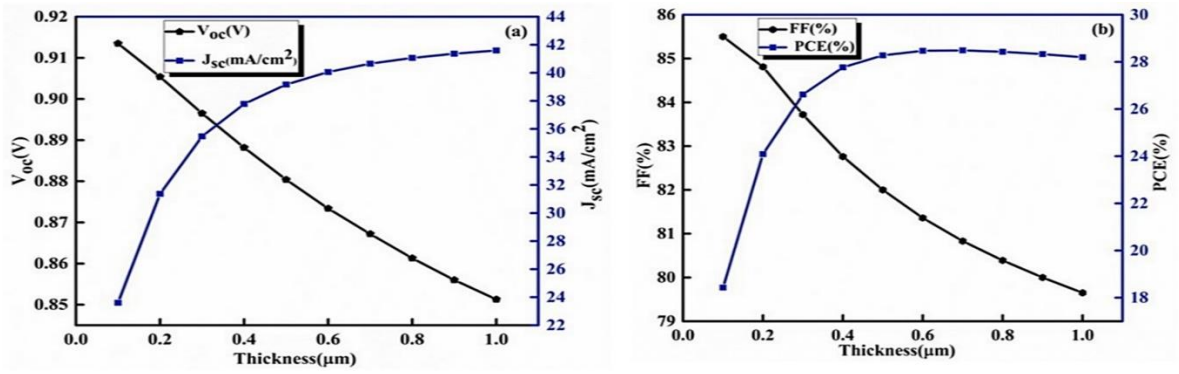

Fig. 4 Variation in thickness of the first absorber layer PbS-TBAI.

The short-circuit current density (Jsc) exhibited a rapid increase with thickness; however, beyond 0.4 μm, the rate of increase slowed considerably. In contrast, the open-circuit voltage (Voc) showed an opposite trend, decreasing as thickness increased, while the fill factor (FF) also declined with further thickening of the absorber. As a result, the overall power conversion efficiency (PCE) rose sharply up to 0.4 μm, then nearly saturated, reaching a maximum of 28.05% at 0.7 μm. These variations can be attributed to a combination of factors, including changes in diffusion length, photon absorption, carrier recombination, and internal resistance. Due to the presence of a secondary absorber layer, the device exhibits distinct behavior compared to a single-absorber architecture. At lower thicknesses, the $Cs_2AgBiBr_6$ layer plays a dominant role, enabling efficient photon absorption. As the PbS–TBAI layer thickness increases, enhanced photon absorption generates more charge carriers, thereby reducing internal resistance and producing a rapid rise in Jsc. Meanwhile, increased recombination and limited diffusion length account for the observed decline in Voc and FF. The net effect is that the improvement in Jsc outweighs these losses up to ~700 nm, resulting in enhanced efficiency that peaks before gradually stabilizing.

5.2 Study of Variation in the thickness of second absorber layer $Cs_2AgBiBr_6$

The second absorber layer is incorporated to enhance the power conversion efficiency (PCE) of the device by capturing radiation transmitted through the PbS–TBAI layer and by establishing favorable band alignment [42]. In addition to photon absorption, this layer plays an important role in aligning energy bands between PbS–TBAI and the Cu_2O hole transport layer (HTL). The effect of varying its thickness, from 0.01 μm to 0.1 μm, is illustrated in Fig. 5. Although changes in thickness exert only a modest influence on photovoltaic parameters, a slight improvement in efficiency is observed. This layer also facilitates effective hole transport by introducing an energetic offset (Fig. 4) that blocks holes from drifting toward the HTL inappropriately, which improves charge selectivity and enhances efficiency. Furthermore, the layer functions as a buffer that supports balanced charge transport across interfaces. In this way, the perovskite layer serves a dual purpose as both an absorber and a buffer layer. The highest efficiency, 25.98%, is achieved at a thickness of 0.09 μm.

Power System Technology
ISSN:1000-3673
Received: 02-11-2025 Revised: 12-12-2025 Accepted: 27-12-2025

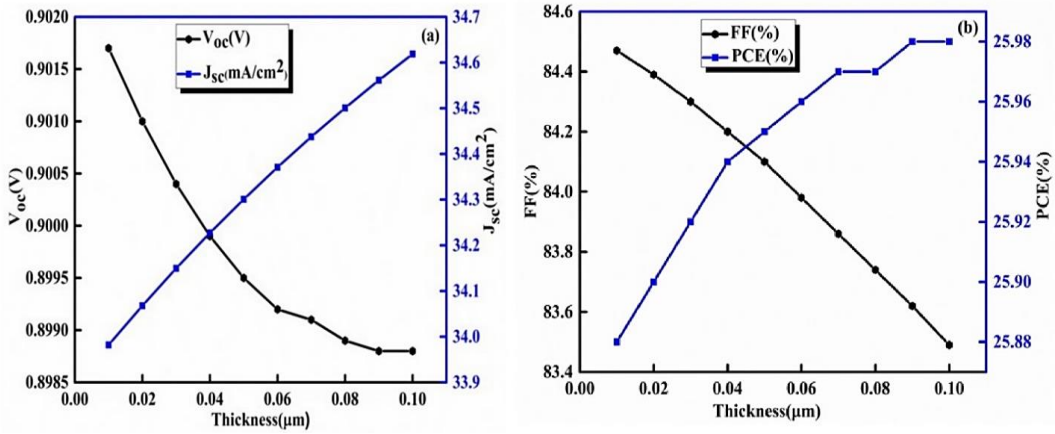

Fig. 5 (a) Variation of V_{oc} and J_{sc} with the thickness of second absorber layer $Cs_2AgBiBr_6$,

(b) Variation of FF and PCE with the thickness of second absorber layer $Cs_2AgBiBr_6$.

5.3 $Cs_2AgBiBr_6/PbS-TBAI$ Interface Defect Density (IDD) variation

The impact of interface defect density on device performance was examined over a range from 10^{10} to 10^{16} cm^{-2}. As shown in Fig. 6, when the interface trap density rises the decline in performance is gradual up to 10^{14} cm^{-2}. Both the Voc and Jsc decreases steadily, which also lowers the power conversion efficiency. At 10^{15} cm^{-2}, the effect becomes much more pronounced. V_{oc}, J_{sc}, PCE show a significant drop, reflecting the stronger role in recombination losses. Interestingly, the FF behaves differently. It continues to rise up to 10^{15} cm^{-2}, likely due to relatively balanced carrier transport and extraction. However, when the trap density reaches 10^{16} cm^{-2}, recombination dominates and resistive effects intensify. This causes the FF to fall along with degradation of overall device performance. Hence, maintain the interface trap density close to 10^{11} cm^{-2} represents both practical and experimentally optimum.

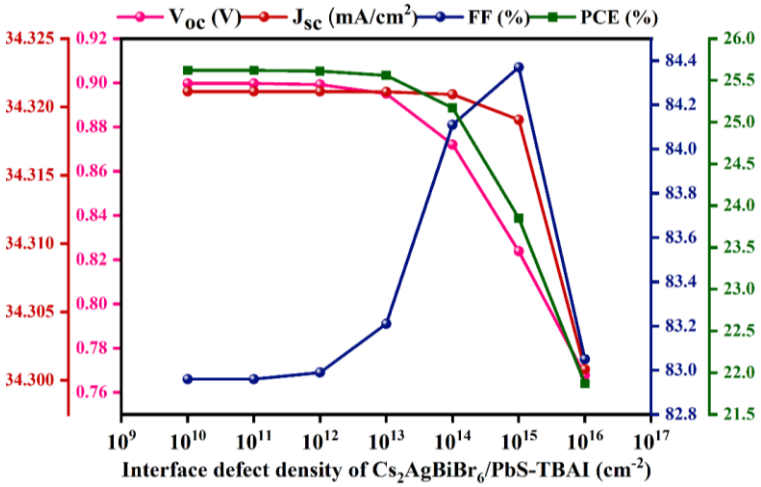

Fig. 6 $Cs_2AgBiBr_6/PbS-TBAI$ IDD variation.

Power System Technology
ISSN:1000-3673
Received: 02-11-2025 Revised: 12-12-2025 Accepted: 27-12-2025

5.4 PbS-TBAI/PCBM Interface Defect Density variation

Interface defect density varies from 10^{10} to 10^{16} cm^{-2}, and an effect is observed in Fig.7. All the cell parameters decrease with increasing defect density at the interface. The efficiency and open circuit voltage decrease very rapidly as the recombination rate increases aggressively with IDD, and charge accumulation at HTL decreases, which decreases PCE and V_{oc} rapidly. Thus the optimize value of IDD is 10^{10} cm^{-2} taken.

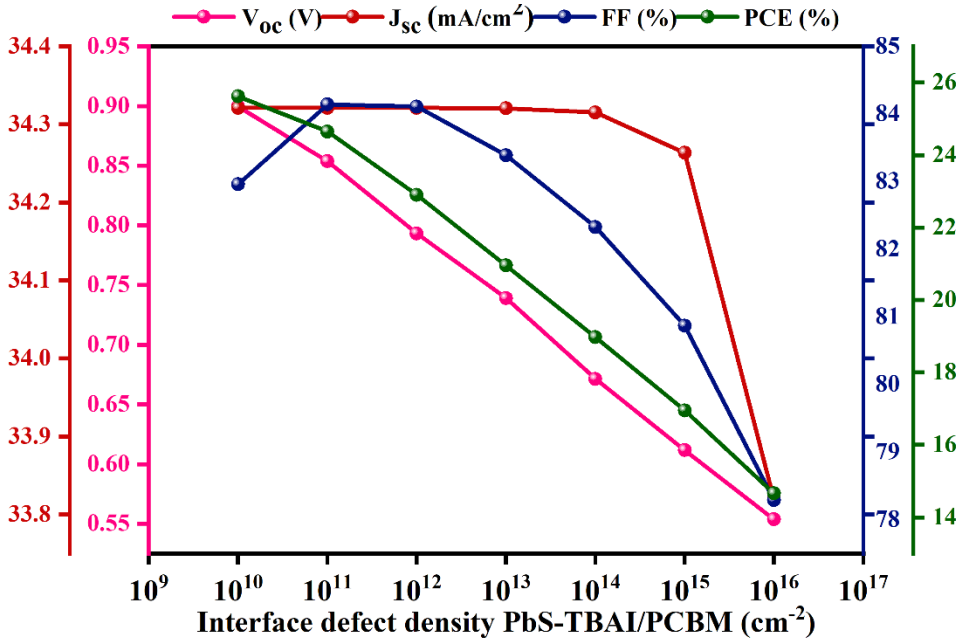

Fig. 7 PbS-TBAI/PCBM IDD variation.

5.6 Impact of Acceptor density of HTL Vs Donor density of ETL Contour Plot

Figure 8 shows the contour plot helps to find suitable values of different parameters to design an optimized structure. As the contour plot is a graphical representation of three dimensional surfaces, it is a better tool to visualize and analyze the performance of solar cell and can identify the optimal values of the variables. Here the values of N_a and N_d are taken from the red zone PCE curve and on caring references it is taken 10^{18} and $10^{20}cm^{-3}$.

5.7 Impact of variation of ETL thickness on performance of solar cells

As ETL is used to transport the electrons generated in absorber layer to the electrodes, so its thickness also affects the performance of cell. An optimal ETL thickness can facilitate efficient charge extraction, reducing recombination losses and increasing solar cell efficiency [43]. The ETL suitable ETL thickness can optimize optical properties, such as transmittance and reflectance, allowing lighter to reach the absorber layer. The Fig. 9 shows the typical the variation of different parameters of solar cell with ETL thickness. Accept FF sthe entire parameters rise with increasing thickness of ETL which varies from 50 nm to 150 nm. The increment is almost slow and uniform but at 80 nm thickness looks more appropriate.

Power System Technology
ISSN:1000-3673
Received: 02-11-2025 Revised: 12-12-2025 Accepted: 27-12-2025

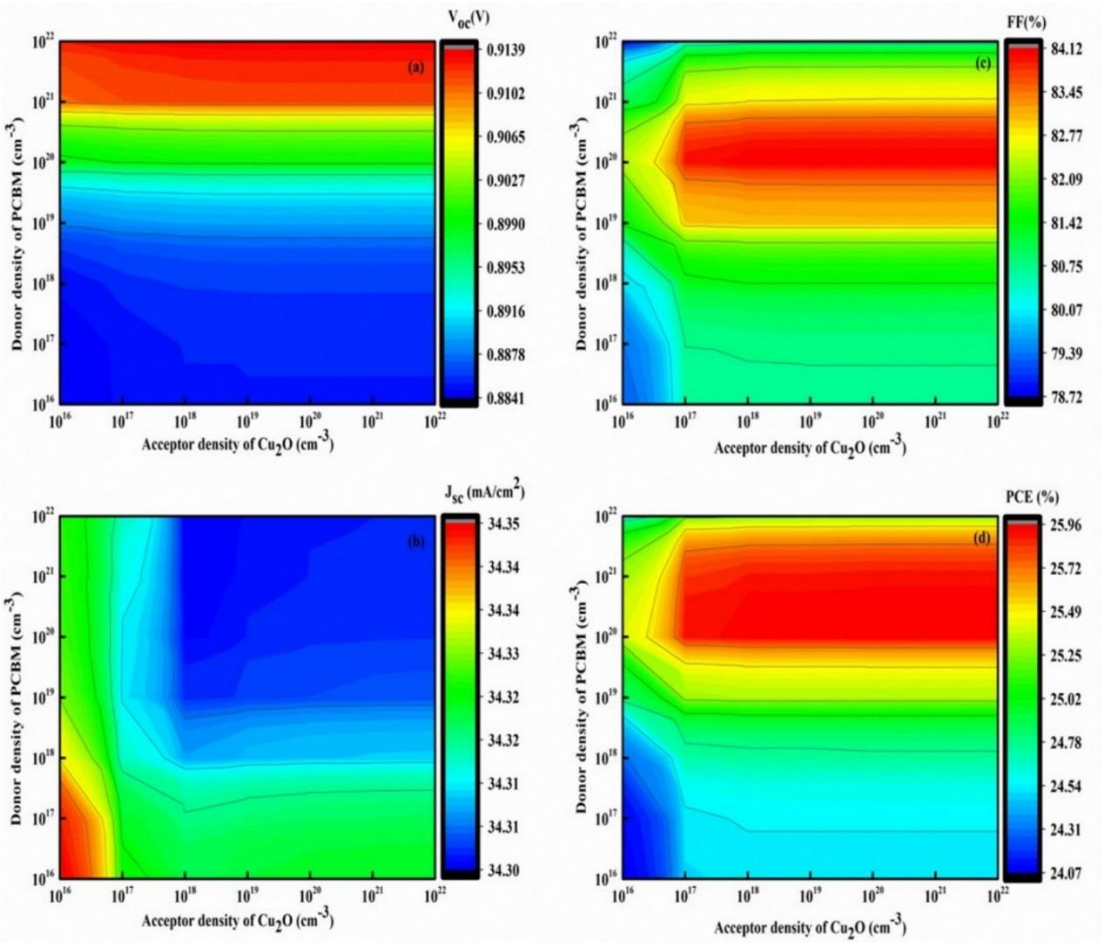

Fig. 8 Impact of Acceptor density of HTL Vs Donor density of ETL Contour Plot.

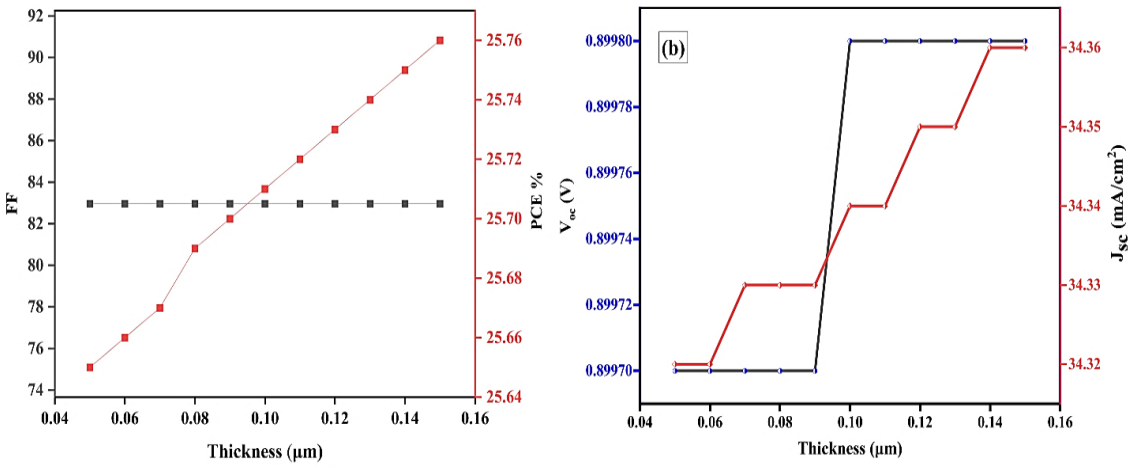

Fig. 9 Variation of electron transport layer (ETL) thickness.

Power System Technology
ISSN:1000-3673
Received: 02-11-2025 Revised: 12-12-2025 Accepted: 27-12-2025

5.8 Impact of variation of total density of PbS-TBAI

The total defect density (N_t) of the absorber material has a significant impact on solar cell performance. An increase in N_t enhances recombination losses, which shortens carrier lifetime and consequently lowers device efficiency [33, 8]. Elevated defect density also promotes non-radiative recombination, further degrading performance. In this study, it is observed that beyond 10^{12} cm^{-3}, the power conversion efficiency (PCE) begins to decline, as shown in Fig. 10.

Although simulations indicate maximum performance at the lowest considered defect density of 10^{10} cm^{-3}, achieving such a low value is difficult in practice for PbS-TBAI quantum dot absorbers. Therefore, considering experimental feasibility, the optimum bulk defect density can be taken around 10^{14} cm^{-3}.

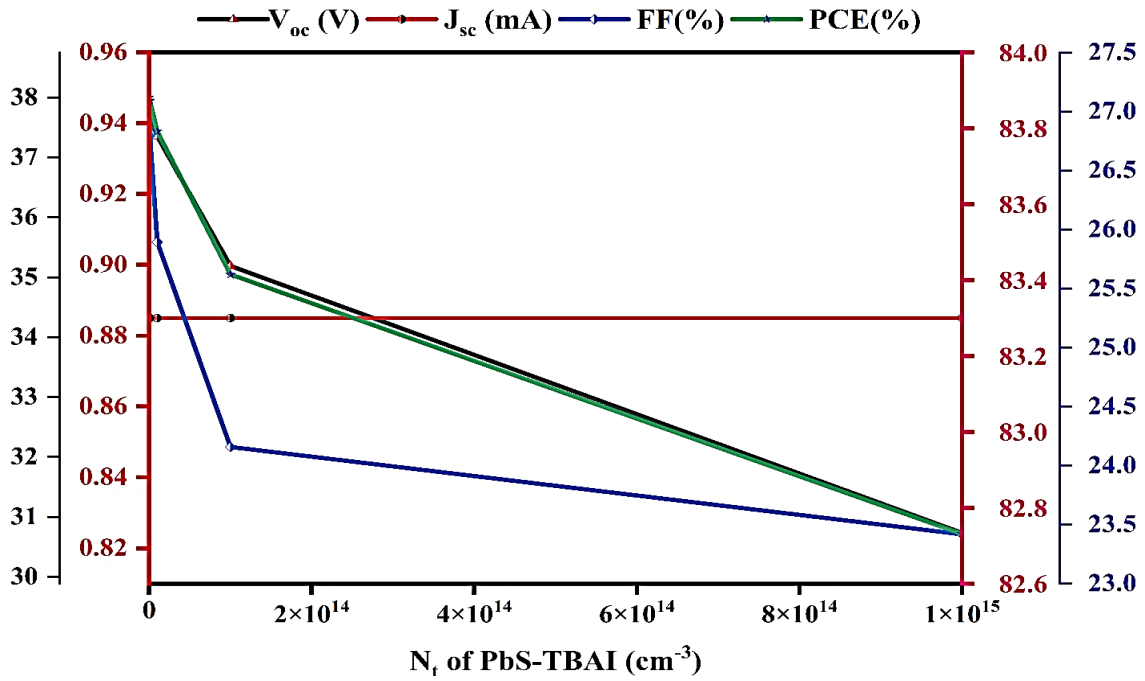

Fig. 10 Impact of variation in total defect density of PbS-TBAI.

5.9 Optimized cell parameters

After analyzing the influence of different parameters on device performance, the optimized values were determined. The optimal thickness of the ETL is 80 nm, with a donor density of 10^{20} cm^{-3}, while the HTL exhibits its best performance with an acceptor density of 10^{18} cm^{-3}. For the absorbers, the thickness of $Cs_2AgBiBr_6$ is optimized at 90 nm, whereas PbS–TBAI shows maximum performance at 700 nm with a defect density (N_t) of 10^{14} cm^{-3}. The optimized interface defect density for both absorbers is found to be 10^{11} cm^{-3} and IDD for PbS-TBAI and PCBM is 10^{10} cm^{-3}. When these optimized parameters are applied in the cell simulation, the resulting performance is remarkable. The quantum efficiency (QE) of the device approaches 100% up to 900 nm, and even at 1000 nm it remains as high as 87.4%, as shown in Fig. 11. This demonstrates that the cell maintains excellent absorption in the infrared region, indicating strong potential for operation under low-light conditions

Power System Technology
ISSN:1000-3673
Received: 02-11-2025 Revised: 12-12-2025 Accepted: 27-12-2025

as well. The final optimized photovoltaic parameters of the designed solar cell are: Voc = 0.8665 V, Jsc = 40.68 mA/cm², FF = 79.16% and PCE = 27.90%.

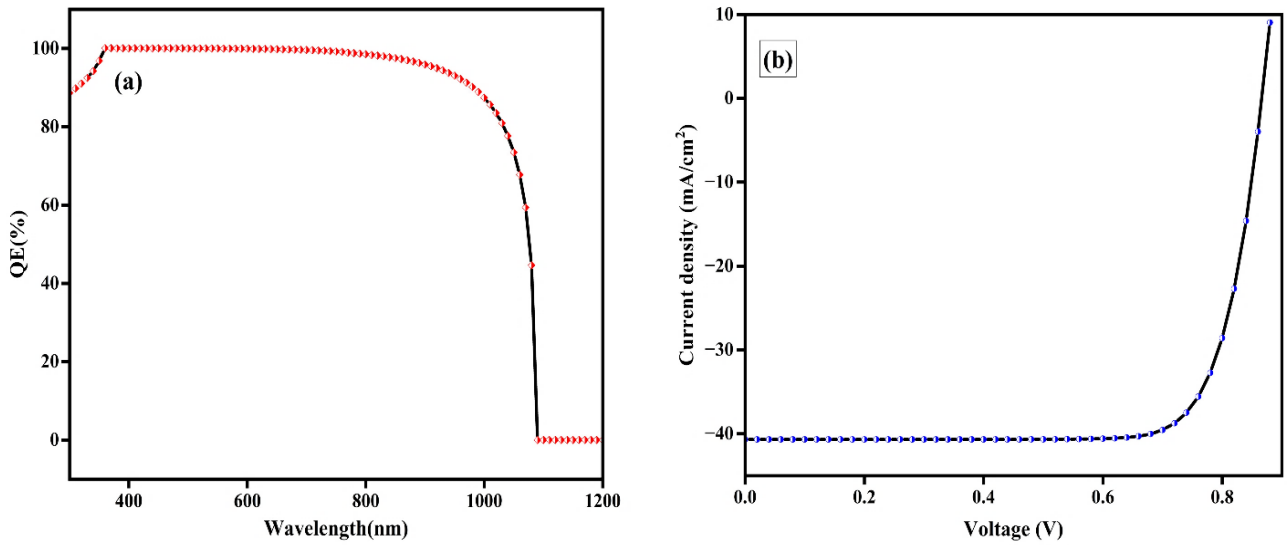

Fig. 11 (a) Quantum efficiency curve of the optimized cell, **(b)** J-V curve of the optimized cell.

Table 2. A comparison study with other cell of the materials used in this work

Solar Cell device architecture	Ref.	V_{oc} (V)	J_{sc} (mA/cm^2)	FF (%)	PCE (%)
FTO/TiO2/Cs2AgBiBr6/SpiroOMeTAD/Ag (Experimental)	[44]	_	_	_	0.7
ITO/MZO/PbS-TBAI/PbS-EDT/Au(Experimental)	[45]	0.620	24.50	62	9.43
ITO/TiO2/PbS-TBAI/HTLs/Au (Simulated)	[46]	0.783	28.50	73.61	16.43
ITO/WS_2/PbS-TBAI/MoO3/Au (simulation)	[42]	0.877	33.789	77.71	23.02
FTO/C_{60}/$Cs_2AgBiBr_6$/MoS_2/Pt (simulation)	[47]	0.84	32.28	85.77	23.49
ITO/PCBM/PbS-TBAI/$Cs_2AgBiBr_6$/Cu_2O/Au (simulation)	This Work	0.8665	40.68	79.16	27.90

6. Conclusion

In the present work, a double perovskite layer ($Cs_2AgBiBr_6$) was introduced above the PbS–TBAI absorber, adjacent to the hole transport layer (HTL). This additional layer serves a dual purpose, functioning both as an absorber and as a buffer, as demonstrated through the performance analysis of

Power System Technology
ISSN:1000-3673
Received: 02-11-2025 Revised: 12-12-2025 Accepted: 27-12-2025

the proposed device architecture. $Cs_2AgBiBr_6$, with its suitable band gap of 1.61 eV, efficiently absorbs intermediate radiation not captured by the PbS–TBAI layer. At the same time, it contributes as a buffer layer by providing a favorable energy offset that facilitates charge transport and ultimately improves efficiency and stability. Incorporation of PCBM as an electron transport material further enhances device performance.

The optimized device structure, $Cu_2O/Cs_2AgBiBr_6/PbS-TBAI/PCBM/ITO$, achieves an efficiency of 27.90% after parameter optimization, as derived from systematic simulation studies and graphical analysis. Although simulation and experimental approaches represent distinct methodologies, they complement each other; thus, the outcomes of this work may serve as a valuable reference for experimentalists seeking to fabricate high-performance solar cells. Looking ahead, the future scope of this research lies in the design of hybrid solar cells employing absorber materials with different band gaps, carefully stacked with appropriate interface engineering, in order to maximize photon absorption across the solar spectrum and further enhance overall device performance.

References

[1] O. B. Ogundipe, S. Akinlabi, and E. T. Akinlabi, "Recent advances in solar photovoltaic technologies: Efficiency, materials, and applications," GSC Adv. Res. Rev., vol. 20, no. 1, pp. 159–175, 2024, doi: 10.30574/gscarr.2024.20.1.0032.

[2] S. Al-Ali, M. Hasan, and Y. Al-Turki, "A review of solar photovoltaic technologies: Developments, challenges and future perspectives," Energy Convers. Manag. X, vol. 23, p. 100564, 2024, doi: 10.1016/j.ecmx.2024.100564.

[3] T. M. Razykov, C. S. Ferekides, and D. Morel, "Solar photovoltaic electricity: Current status and future prospects," Renew. Sustain. Energy Rev., vol. 176, p. 113119, 2023, doi: 10.1016/j.rser.2023.113119.

[4] M. A. Green, E. D. Dunlop, J. Hohl-Ebinger, M. Yoshita, N. Kopidakis, and A. W. Y. Ho-Baillie, "Solar cell efficiency tables (Version 63)," Prog. Photovoltaics Res. Appl., vol. 31, no. 1, pp. 3–16, 2023, doi: 10.1002/pip.3661.

[5] M. A. Green and E. D. Dunlop, "Progress and challenges for CdTe and CIGS thin-film solar cells," Joule, vol. 8, no. 2, pp. 245–260, 2024, doi: 10.1016/j.joule.2024.01.004.

[6] W. Shockley and H. J. Queisser, "Detailed balance limit of efficiency of p–n junction solar cells," J. Appl. Phys., vol. 32, pp. 510–519, 1961, doi: 10.1063/1.1736034.

[7] A. J. Nozik, "Multiple exciton generation in semiconductor quantum dots," Chem. Phys. Lett., vol. 457, no. 1–3, pp. 3–11, 2008, doi: 10.1016/j.cplett.2008.03.026.

[8] M. A. Green, "Third generation photovoltaics: Advanced concepts for high efficiency," Phys. E Low-dimensional Syst. Nanostructures, vol. 148, p. 115602, 2023, doi: 10.1016/j.physe.2022.115602.

[9] I. J. Kramer and E. H. Sargent, "Colloidal quantum dot photovoltaics: Materials, devices, and progress," Chem. Rev., vol. 123, no. 3, pp. 1673–1751, 2023, doi:

Power System Technology
ISSN:1000-3673
Received: 02-11-2025 Revised: 12-12-2025 Accepted: 27-12-2025

10.1021/acs.chemrev.2c00654.

[10] H. J. Snaith, "Present status and future prospects of perovskite photovoltaics," Nat. Energy, vol. 9, no. 1, pp. 1–10, 2024, doi: 10.1038/s41560-023-01358-5.

[11] V. I. Klimov, "Nanocrystal quantum dots: From fundamental photophysics to multicolor displays and solar cells," Chem. Rev., vol. 123, no. 3, pp. 1343–1413, 2023, doi: 10.1021/acs.chemrev.2c00671.

[12] X. Huang, S. Han, W. Huang, and X. Liu, "Enhancing solar cell efficiency: the search for luminescent materials as spectral converters," Chem. Soc. Rev., vol. 42, no. 1, pp. 173–201, 2013.

[13] N. Shah et al., "A Review of Third Generation Solar Cells," Processes, vol. 11, no. 6, 2023, doi: 10.3390/pr11061852.

[14] X. Lan, O. Voznyy, and E. H. Sargent, "Advances in colloidal quantum dot solar cells with infrared response and low-light performance," Adv. Energy Mater., vol. 12, no. 5, p. 2101867, 2022, doi: 10.1002/aenm.202101867.

[15] D. Zhitomirsky, I. J. Kramer, and E. H. Sargent, "Colloidal quantum dot photovoltaics for low-light and indoor energy harvesting," Nat. Energy, vol. 8, no. 3, pp. 289–298, 2023, doi: 10.1038/s41560-022-01199-2.

[16] A. Memari, M. Javadian Sarraf, S. J. Seyyed Mahdavi Chabok, and L. Motevalizadeh, "Comprehensive guidance for optimizing the colloidal quantum dot (CQD) Perovskite solar cells: experiment and simulation," Sci. Rep., vol. 13, no. 1, 2023, doi: 10.1038/s41598-023-43933-x.

[17] R. Wang and J. Tang, "Bandgap engineering and spectral broadening in PbS quantum dot solar cells," ACS Energy Lett., vol. 8, no. 1, pp. 112–121, 2023, doi: 10.1021/acsenergylett.2c02345.

[18] W. Wang, M. O. Tade, and Z. Shao, "Research progress of perovskite materials in photocatalysis-and photovoltaics-related energy conversion and environmental treatment," Chem. Soc. Rev., vol. 44, no. 15, pp. 5371–5408, 2015.

[19] M. Burgelman, P. Nollet, and S. Degrave, "Modelling polycrystalline semiconductor solar cells," Thin Solid Films, vol. 361, pp. 527–532, 2000.

[20] M. K. Hossain and F. H. Alharbi, "Numerical simulation and optimization of emerging solar cell devices using SCAPS-1D," Opt. Mater. (Amst)., vol. 142, p. 113829, 2023, doi: 10.1016/j.optmat.2023.113829.

[21] H. Zhang, X. Lan, and E. H. Sargent, "Dual-absorber perovskite–PbS quantum dot solar cells for broadband light harvesting," Energy Environ. Sci., vol. 17, no. 3, pp. 812–821, 2024, doi: 10.1039/D3EE04112A.

[22] K. A. Bush, A. F. Palmstrom, and M. D. McGehee, "Principles of spectral complementarity in

Power System Technology
ISSN:1000-3673
Received: 02-11-2025 Revised: 12-12-2025 Accepted: 27-12-2025

tandem solar cells," Joule, vol. 6, no. 2, pp. 350–365, 2022, doi: 10.1016/j.joule.2021.12.012.

[23] J. Tong, Y. Liu, and E. H. Sargent, "Tandem solar cells integrating perovskites and quantum dots," Nat. Energy, vol. 8, no. 5, pp. 471–480, 2023, doi: 10.1038/s41560-023-01245-z.

[24] S. Li, Y. Cao, W. Li, and Z. Bo, "A brief review of hole transporting materials commonly used in perovskite solar cells," Rare Met., vol. 40, no. 10, pp. 2712–2729, 2021, doi: 10.1007/s12598-020-01691-z.

[25] P. Dubey, B. K. Pandey, and D. K. Dwivedi, "Optik Contribution towards the selection of electron and hole transport layers for the development of highly efficient PbS colloidal quantum dot solar cell," Optik (Stuttg)., vol. 266, no. December 2021, p. 169600, 2022, doi: 10.1016/j.ijleo.2022.169600.

[26] A. Yousfi et al., "Numerical Simulation of High-Efficiency Double-Absorber Layer Perovskite Solar Cells Using SCAPS- 1D and MATLAB PV Models," Trans. Electr. Electron. Mater., pp. 366–379, 2025, doi: 10.1007/s42341-025-00606-y.

[27] M. K. Hossain et al., "Design and Simulation of Cs2BiAgI6 Double Perovskite Solar Cells with Different Electron Transport Layers for Efficiency Enhancement," Energy and Fuels, vol. 37, no. 5, pp. 3957–3979, 2023, doi: 10.1021/acs.energyfuels.3c00181.

[28] M. I. Nanostructures, "Enhancement of Quantum Dot Solar Cell Efficiency : Implementation of Enhancement of Quantum Dot Solar Cell Efficiency : Implementation of Multilayer InAs Nanostructures," no. July, 2023, doi: 10.5281/zenodo.15298012.

[29] N. Rai, S. Rai, P. K. Singh, P. Lohia, and D. K. Dwivedi, "Analysis of various ETL materials for an efficient perovskite solar cell by numerical simulation," J. Mater. Sci. Mater. Electron., vol. 31, no. 19, pp. 16269–16280, 2020, doi: 10.1007/s10854-020-04175-z.

[30] K. Neupane et al., "Empowering rubidium-based halide PSCs: A deep dive into ETL material performance," J. Phys. Chem. Solids, vol. 207, no. May, 2025, doi: 10.1016/j.jpcs.2025.112897.

[31] S. Bhattarai et al., "TCAD study of CIGS/CZTS double absorber solar cells for high-efficiency photovoltaic applications," J. Opt., 2025, doi: 10.1007/s12596-025-02769-6.

[32] A. K. Datta et al., "Theoretical insights into lead-free planer Cs2AuBiCl6 based double perovskite solar cells with various charge transport layers via numerical analysis," J. Phys. Chem. Solids, vol. 206, no. September 2024, p. 112872, 2025, doi: 10.1016/j.jpcs.2025.112872.

[33] A. H. Slavney and H. I. Karunadasa, "Halide double perovskites: Electronic structure and photovoltaic potential of Cs2AgBiBr6," J. Mater. Chem. A, vol. 11, no. 5, pp. 2143–2152, 2023, doi: 10.1039/D2TA08921A.

[34] F. Liu, Z. Zhou, and C. Zhang, "Electronic properties of ITO and PCBM layers for photovoltaic device simulation," Opt. Mater. (Amst)., vol. 111, p. 110584, 2021, doi: 10.1016/j.optmat.2020.110584.

Power System Technology
ISSN:1000-3673
Received: 02-11-2025 Revised: 12-12-2025 Accepted: 27-12-2025

[35] J. Tang and E. H. Sargent, “Infrared colloidal quantum dot photovoltaics: Materials and device physics,” Adv. Mater., vol. 34, no. 1, p. 2104487, 2022, doi: 10.1002/adma.202104487.

[36] T. Minami, “Oxide semiconductor materials for solar cells,” Thin Solid Films, vol. 516, no. 17, pp. 5822–5828, 2020, doi: 10.1016/j.tsf.2007.12.039.

[37] J. Nelson, The Physics of Solar Cells. Imperial College Press, 2003. doi: 10.1142/p276.

[38] M. A. Green, “How solar cell bandgaps relate to the solar spectrum,” Prog. Photovoltaics Res. Appl., vol. 31, no. 7, pp. 637–646, 2023, doi: 10.1002/pip.3725.

[39] P. K. Patel, “Device simulation of highly efficient eco - friendly - perovskite solar cell,” Sci. Rep., pp. 1–11, 2021, doi: 10.1038/s41598-021-82817-w.

[40] K. A. Bush, A. F. Palmstrom, and M. D. McGehee, “Intermediate band gaps and tandem architectures for enhanced solar spectrum utilization,” Joule, vol. 6, no. 2, pp. 350–365, 2022, doi: 10.1016/j.joule.2021.12.012.

[41] M. A. Green, “Reducing thermalization losses in advanced solar cell architectures,” Prog. Photovoltaics Res. Appl., vol. 31, no. 9, pp. 901–910, 2023, doi: 10.1002/pip.3751.

[42] S. Pandey, B. Kumar, P. Km, P. Mishra, and J. Gupta, “Performance optimization of the PbS - quantum dot solar cell by the selection of suitable ETL through numerical simulation,” Opt. Quantum Electron., vol. 57, no. 241, 2025.

[43] K. P. Mishra, B. K. Pandey, and S. Pandey, “Unveiling the potential of FASnI3 solar cells through advanced charge transport materials: A SCAPS-1D perspective,” J. Alloys Compd., vol. 1006, no. September, p. 176283, 2024, doi: 10.1016/j.jallcom.2024.176283.

[44] P. Fan et al., “Single-source vapor-deposited Cs2AgBiBr6 thin films for lead-free perovskite solar cells,” Nanomaterials, vol. 9, no. 12, pp. 1–13, 2019, doi: 10.3390/nano9121760.

[45] X. Zhang, C. Hägglund, and E. M. J. Johansson, “Highly efficient, transparent and stable semitransparent colloidal quantum dot solar cells: A combined numerical modeling and experimental approach,” Energy Environ. Sci., vol. 10, no. 1, pp. 216–224, 2017, doi: 10.1039/c6ee02824a.

[46] S. Kumar, P. Bharti, and B. Pradhan, “Performance optimization of efficient PbS quantum dots solar cells through numerical simulation,” Sci. Rep., vol. 13, no. 1, p. 10511, 2023, doi: 10.1038/s41598-023-36769-y.

[47] N. Jaiswal, D. Kumari, R. Shukla, and S. K. Pandey, “Design and Performance Optimization of Eco-friendly Cs2AgBiBr6 Double Perovskite Solar Cell,” J. Electron. Mater., vol. 52, no. 12, pp. 7842–7849, 2023, doi: 10.1007/s11664-023-10705-2.